1993

Parametric Studies of the Formation of Calcareous Deposits on Cathodically Protected Steel in Seawater

J. F. Yan
Texas A & M University - College Station

Ralph E. White
University of South Carolina - Columbia, white@cec.sc.edu

R. B. Griffin
Texas A & M University - College Station

Publication Info

Journal of the Electrochemical Society, 1993, pages 1275-1280.

Parametric Studies of the Formation of Calcareous Deposits on Cathodically Protected Steel in Seawater

J.-F. Yan*

Center for Electrochemical Engineering, Department of Chemical Engineering, Texas A&M University, College Station, Texas 77843-3122

R. E. White**

Department of Chemical Engineering, University of South Carolina, Columbia, South Carolina 29208

R. B. Griffin

Department of Mechanical Engineering, Texas A&M University, College Station, Texas 77843-1292

ABSTRACT

A first principle mathematical model has been used to study the effects of ocean environment and cathodic protection on the formation of calcareous deposits and their ability to reduce the cathodic current density. These parameters include applied potential, rotation speed, temperature, salinity, and depth. The results showed the applied potential strongly influences the formation of calcareous deposits and their ability to reduce the cathodic current density. Among the environmental factors, rotation speed has the most influence on the cathodic current density. Salinity slightly influences the cathodic current density over the range of interest. Temperature is much more influential than salinity on the ability of calcareous deposits to reduce the cathodic current density. The results from modeling showed the formation rate of calcareous deposits is much lower at 5°C than at room temperature. The depth is very critical not only to cathodic current density but also to the formation of calcareous deposits in seawater. The formation of calcareous deposits would be expected to be slower and the deposits would contain more $Mg(OH)_2$ in deep water.

In the first part of this research, a first principles mathematical model was presented for the formation of calcareous deposits on cathodically protected steel in seawater.[1] This model and the main results of the model will be summarized in the next section. The results from the model are helpful in understanding the mechanism of the formation of calcareous deposits on cathodically protected steel in seawater and their effects on cathodic protection (CP) systems. The model is also capable of predicting the changes in current density and composition of the deposits with time. Since one of the purposes of this research is to predict the conditions necessary for the formation and the maintenance of calcareous films on structural steels in deep ocean water, the parametric studies are necessary to understand the effects of various parameters on the formation of calcareous deposits.

The model has been used to examine how the physical and chemical properties of seawater and cathodic protection parameters influence the formation of calcareous deposits and their ability to lower the cathodic current density. The results from a previous study[1] indicate that the chemical (oxygen concentration and pH) and physical properties (temperature) of seawater are important for the formation of calcareous deposits. Since most chemical and physical properties of seawater depend on salinity and temperature, these two parameters are varied in this study. Also, the effect of depth on these parameters is included. In addition to the parameters mentioned above, the sea current (rotation speed), and the applied potential are also included in the parametric studies. All the parameters listed in Ref. 1 are used in these studies, except for those depending on the environmental conditions (temperature, salinity, and depth). These environment-dependent parameters are listed in Tables I-V and will be mentioned in the individual section.

Summary of the Model and Results

The main electrochemical reactions that occur during the corrosion of steel structures in seawater are the oxidation of iron

$$Fe \rightarrow Fe^{2+} + 2e^- \quad [1]$$

the reduction of oxygen

$$O_2 + 2H_2O + 4e^- \rightarrow 4\ OH^- \quad [2]$$

and the evolution of hydrogen

$$2H_2O + 2e^- \rightarrow H_2 + 2\ OH^- \quad [3]$$

Under cathodic protection, the oxidation of iron is prohibited by supplying electrons to the metal structure to be protected by means of sacrificial anodes or impressed current.[2]

The high concentration of OH^- ions generated by the electrochemical reactions on the electrode surface causes the precipitations of $Mg(OH)_2$

$$Mg^{2+} + 2\ OH^- \rightarrow Mg(OH)_2\downarrow \quad [4]$$

Also, the production of OH^- ions on the electrode surface changes the inorganic carbon equilibria in the adjacent seawater and facilitates the following buffering reaction[3]

$$OH^- + HCO_3^- \rightleftarrows H_2O + CO_3^{2-} \quad [5]$$

As a result, $CaCO_3$ also precipitates

$$Ca^{2+} + CO_3^{2-} \rightarrow CaCO_3\downarrow \quad [6]$$

The calcareous deposits are assumed to be a mixture of $CaCO_3$ and $Mg(OH)_2$ in the model.

Our experimental results[1] showed that calcareous deposits block the active surface area available for the electrochemical reactions and consequently reduce the current density to the specimen during CP. Thus, surface coverage, defined as the ratio of total surface area covered by the porous deposits to the total electrode surface area, is used to determine the formation rate of calcareous deposits. The dependence of surface coverage (θ) with time (t) is expressed by the following equation

$$\frac{\partial\theta}{\partial t} = -\frac{1}{(1-\epsilon_d)\delta}\left(\frac{R''_{Ca^{2+}}MW_{CaCO_3}}{\rho_{CaCO_3}} + \frac{R''_{Mg^{2+}}MW_{Mg(OH)_2}}{\rho_{Mg(OH)_2}}\right) \quad [7]$$

The current density due to electrochemical reaction j (i_j) is corrected to account for the decrease in active surface area by the following equation

$$i_j = [(1-\theta) + \epsilon_d\theta]j_j \quad [8]$$

* Electrochemical Society Student Member.
** Electrochemical Society Active Member.

where the local current density (i_j) generated by electrochemical reaction j is assumed to be described by a Butler-Volmer equation.[1,4-6] The total current density is found by summing the individual current densities[7]

$$i_T = \sum_{j=1}^{NR} i_j \qquad [9]$$

The deposit porosity (ϵ_d) is used to express the protectiveness of calcareous deposits such that the current density (i_j) is expected to approach to a steady state, nonzero value as the surface coverage (θ) approaches 1.0.

The eleven unknowns (concentrations of nine components in seawater, solution potential, and surface coverage) were solved by using Newman's BAND(J) subroutine,[8] which is based on the finite difference method.[9] The implicit method[9] was used to handle the time step. A case study using the parameters estimated at 25°C and 35 ppt salinity was presented in Ref. 1 and the results are summarized below.

The predicted concentration profile of OH^- ions in the diffusion layer indicates that the formation of calcareous deposits is due to the higher pH on the electrode surface (≈9.9), which causes the precipitation of $Mg(OH)_2$. The pH is about 8.2 in the bulk solution. Also, the higher concentration of OH^- ions facilitates the buffering reaction and consequently increases the concentration of CO_3^{2-} ions by a factor of about eight times higher than that in the bulk solution. As a result, the formation of $CaCO_3$ is increased.

The current density was found to drop quickly at first and to continue to decrease with time but at a much slower rate. The initial almost instantaneous drop in the current density (in seconds) is attributed to the depletion of oxygen on the electrode surface; and, the second decrease in the current density is due to the increasing surface coverage caused by the formation of the calcareous deposits on the electrode surface.

The calcareous deposits were predicted to contain mostly $CaCO_3$. However, the initial deposits were expected to contain more $Mg(OH)_2$ than $CaCO_3$ because of the very high pH on the electrode surface before the depletion of oxygen, as mentioned above.

Effect of Applied Potential

The parameters listed in Ref. 1 are used in studying the effect of applied potential. All the parameters are assumed to be independent of the applied potential. Figure 1 shows

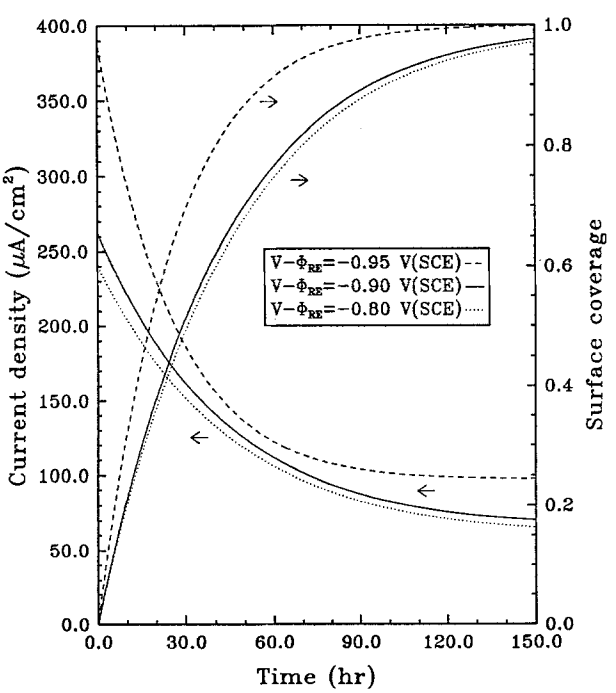

Fig. 1. Effect of applied potential on the change in current density and surface coverage with time (50 rpm, 25°C, 35 ppt salinity).

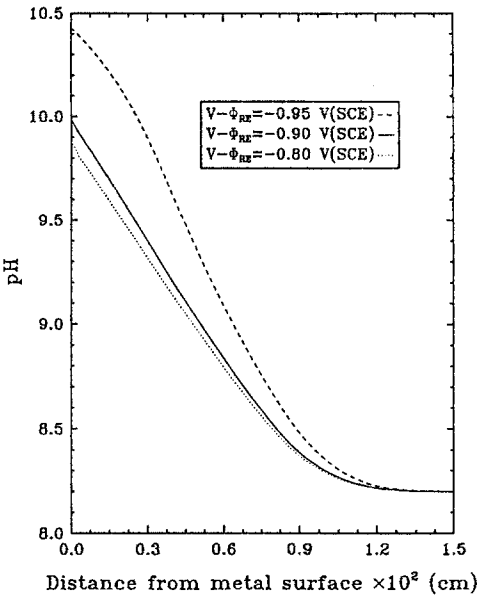

Fig. 2. Effect of applied potential on the change in pH distribution inside the diffusion layer after 150 h (50 rpm, 25°C, 35 ppt salinity).

the applied potential's influence on the surface coverage and current density. The influence of electrode potential comes from the change of overpotential. The higher the overpotential on the electrode surface, the higher cathodic current density, which causes a higher concentration of OH^- on the electrode surface and results in a higher rate of formation of calcareous deposits, as shown in Fig. 2. Moreover, the higher pH is favorable for the formation of $Mg(OH)_2$. The deposits formed at more negative applied potentials would be expected to have low ratio of $CaCO_3$ to $Mg(OH)_2$. This finding confirms the composition analysis of calcareous coatings by Humble[10] that the content of Mg increases with increasing current density.

Lee and Ambrose[11] claimed that calcareous deposits are capable of decreasing the rate of the oxygen reduction reaction by functioning as a barrier to oxygen transport; however, their influence on hydrogen evolution is limited apparently because this reaction is activation controlled. Thus, they concluded that the applied potential has little influence on the decrease of the current density. However, our results in Fig. 1 show that the applied potential has a substantial influence on the formation of calcareous deposits as well as the decrease in the cathodic current density. This is true because the calcareous deposits reduce not only the transport rate of oxygen to the substrate surface but also the active surface area available for the electrochemical reactions. This results in a decrease in the cathodic current density for both oxygen reduction and hydrogen evolution.

Wolfson and Hartt[12] found that the steady-state current density needed to maintain an applied potential of −1.03 V (SCE) was less than that for −0.93 V (SCE), and they concluded that the calcareous deposits formed at −1.03 V (SCE) were probably more protective than those formed at −0.93 V (SCE). Figure 1 shows that the steady-state current density needed to maintain an applied potential of −0.95 V (SCE) is higher than those for −0.90 and −0.80 V (SCE). This inconsistency with Wolfson and Hartt's experimental results may be due to using a constant deposit porosity (ϵ_d = 0.25) and a constant deposit thickness (δ = 10 μm) in the modeling. Before this issue can be solved, more experimental data which includes values for the porosity and thickness of the deposits are needed.

The experimental results from Ref. 13 showed that the initial deposits do not completely cover the electrode surface because of the decreasing pH on the electrode surface. In order to polarize quickly steel structures in seawater and obtain more protective initial deposits, a more negative ap-

plied potential would be helpful. Currently, an optimum cathodic protection design using sacrificial anodes is achieved by inducing a high current density immediately upon immersion.[14] This approach promotes rapid polarization and formation of calcareous deposits during the initial stage of CP and reduces the current density necessary to maintain long term CP.

From the point of view of economy, to apply a higher potential requires increasing the number of sacrificial anodes or electricity supplied from an impressed-current transformer/rectifier. This means that the operating cost rises. Therefore, it may be misleading to say that a more negative applied potential is always favorable for better cathodic protection performance and fast formation of calcareous deposits. In practice, an optimal applied potential could be determined by considering the balance between the protectiveness of calcareous deposits and the operating costs, *i.e.*, the number of sacrificial anodes or the current output from a rectifier.

Effect of Rotation Speed

The parameters listed in Ref. 1 are used in studying the effect of rotation speed. All the parameters are assumed to be independent of the rotation speed except the thickness of the diffusion layer. Higher rotation speeds lead to more dissolved oxygen on the electrode surface and hence generate higher cathodic current densities, as shown in Fig. 3. The surface coverage, however, does not increase at higher rotation speeds. The increase in the current density for higher rpm values is related to the thinner diffusion layer, which results in a higher oxygen transfer rate. However, the thinner diffusion layer also promotes the diffusion rate of OH^- ions back to the bulk solution. Also, the mass flux of HCO_3^- ions due to convection increases at higher rotation speeds and consumes more OH^- ions in the homogeneous reaction, Eq. 5. Consequently, the pH on the electrode surface does not increase much, as shown in Fig. 4. As a result, a higher rotation speed makes little contribution to the formation of calcareous deposits even though the total current density increases considerably.

Lee and Ambrose[11] found that the difference in the percentage of current decrease caused by deposit formation between 500 and 1000 rpm was negligible and they concluded that the increase in electrode rotation speed has little influence on the pH near the electrode surface, and therefore, little influence on deposit formation. The results in Fig. 3 quantitatively confirm their statement that the rotation speed has no effect on the pH near the electrode surface. The results in Fig. 3 also confirm the conclusion by Wolfson and Hartt[12] that the current density required to maintain a particular potential increases with velocity.

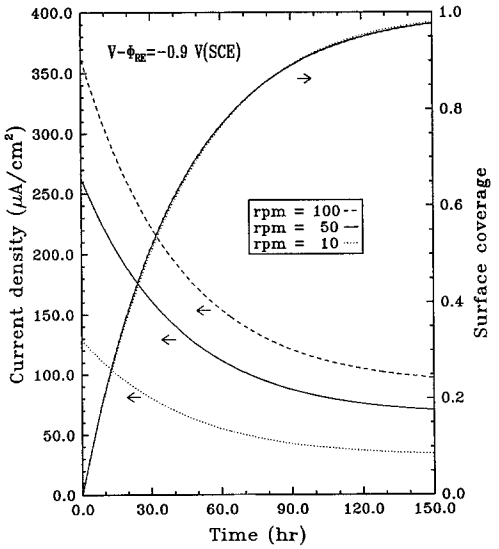

Fig. 3. Effect of rotation speed on the change in current density and surface coverage with time [−0.9 V (SCE), 25°C, 35 ppt salinity].

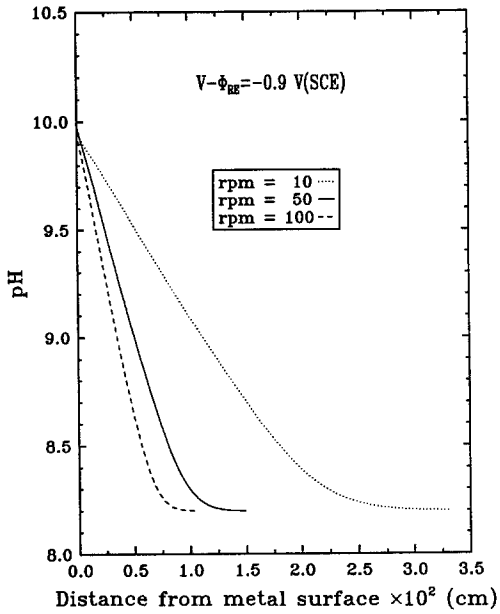

Fig. 4. Effect of rotation speed on the chqange in pH distribution inside the diffusion layer after 150 h [−0.9 V (SCE), 25°C, 35 ppt salinity].

Previous work showed that high rotation speed did not remove the calcareous deposits from a rotating cylinder electrode.[15] However, the higher rotation speed might be harmful to the nucleation and growth of $CaCO_3$ and $Mg(OH)_2$ crystals. Therefore, a high velocity has no advantage in the formation of calcareous deposits.

The results in Fig. 3 and 4 also indicate that to increase the formation rate of calcareous deposits, generating a higher current density as well as maintaining a higher pH on the electrode surface is necessary.

The results shown on Fig. 3 and 4 are obtained with the same deposit thickness, 10 μm. Previous work showed that the deposit thickness decreases with increasing solution velocity.[12] To obtain a better prediction, the effect of the deposit thickness should be taken into consideration.

Effect of Temperature

The composition (except for the solid contents) and the transport properties of seawater are sensitive to temperature. The thermodynamics and kinetics of the homogeneous and precipitation reactions also depend on tempera-

Table I. Transport properties and the concentrations of the components in seawater at temperatures of 25, 15, and 5°C (salinity = 35 ppt).

Parameter	25°C	15°C	5°C
$c_{O_2} \times 10^{7}$ [a] (mol/cm^3)	2.11	2.54	3.17
$c_{H_2} \times 10^{10}$ [a] (mol/cm^3)	6.69	7.09	7.70
$c_{OH^-} \times 10^{9}$ [b] (mol/cm^3)	1.60	1.41	1.20
$c_{CO_3^{2-}} \times 10^{6}$ [b] (mol/cm^3)	0.21	0.65	2.28
$c_{HCO_3^-} \times 10^{6}$ [b] (mol/cm^3)	1.51	3.37	8.05
$D_{O_2} \times 10^{5}$ [c] (cm^2/s)	2.90	2.11	1.61
$D_{H_2} \times 10^{5}$ [c] (cm^2/s)	6.28	4.78	3.49
$D_{OH^-} \times 10^{5}$ [d] (cm^2/s)	5.27	4.02	2.93
$D_{Mg^{2+}} \times 10^{5}$ [d] (cm^2/s)	0.71	0.54	0.39
$D_{Ca^{2+}} \times 10^{5}$ [d] (cm^2/s)	0.79	0.60	0.44
$D_{CO_3^{2-}} \times 10^{5}$ [d] (cm^2/s)	0.96	0.73	0.53
$D_{HCO_3^-} \times 10^{5}$ [d] (cm^2/s)	1.19	0.90	0.66
$D_{Na^+} \times 10^{5}$ [d] (cm^2/s)	1.34	1.02	0.74
$D_{Cl^-} \times 10^{5}$ [d] (cm^2/s)	2.03	1.55	1.13
$\rho_o \times 10^{3}$ [a] (kg/cm^3)	1.023	1.026	1.028
$\nu \times 10^{2}$ [a] (cm^2/s)	0.93	1.18	1.56

[a] Predicted from the equations in Ref. 28.
[b] Predicted from the equations in Ref. 29.
[c] Chosen arbitrarily and adjusted to 15 and 5°C by Eq. 4 in Ref. 30.
[d] Taken from Ref. 31 and adjusted to 15 and 5°C by Eq. 4 in Ref. 30.

Table II. Parameters of the precipitation reactions and the homogeneous reaction at temperatures of 25, 15, and 5°C (salinity = 35 ppt).

Parameter	25°C	15°C	5°C
$K_{sp,CaCO_3} \times 10^{13}$ [a] (mol^2/cm^6)	9.14	9.78	10.4
$K_{sp,Mg(OH)_2} \times 10^{19}$ [b] (mol^3/cm^9)	4.50	3.65	2.80
$k_{CaCO_3} \times 10^{13}$ [c] ($mol/cm^2 \cdot s$)	11.3	9.77	4.0
$k_{Mg(OH)_2} \times 10^{7}$ [b] ($cm^7/mol^2 \cdot s$)	3.7	2.85	2.0
m_{CaCO_3} [c]	1.7	1.0	0.4
$K_{eq} \times 10^{-8}$ [a] (cm^3/mol)	0.84	1.36	2.36

[a] Predicted from Ref. 29.
[b] Taken from Ref. 27 and adjusted to 15°C.
[c] Taken from Ref. 25 and adjusted to 15°C.

ture. Tables I and II list these parameters as a function of temperature at 35 ppt salinity. The rest of the parameters have the same values as in Ref. 1. The computed results of the effect of temperature on current density and surface coverage at 25, 15, and 5°C are shown in Fig. 5, which is consistent quantitatively with the previous work[16,17] that showed that the calcareous deposits formed at low temperatures afford less protection.

In spite of the increase in the oxygen bulk concentration at low temperatures, the mass-transfer of oxygen does not increase significantly because of the lower diffusion coefficient under these conditions. Hence, the initial current density only slightly decreases at low temperatures, as shown in Fig. 5. However, the surface coverage at low temperatures is much lower than that at room temperature. This can be explained from the smaller reaction constant ($k_{sp,CaCO_3}$) and reaction order (m_{CaCO_3}) at low temperatures, as listed in Table II. The higher solubility constant of $CaCO_3$ ($k_{sp,CaCO_3}$) at low temperatures also reduces the formation rate of $CaCO_3$.

There has been considerable discussion associated with the low formation rate of calcareous deposits at low temperatures. It was reported that the calcareous deposits are Mg^{2+}-rich when grown in cold water, an the protectiveness of this porous layer is poor, due to higher porosity,[16,18] and the calcareous deposits grown at low temperature may have semiconductive properties such that the electrochemical reactions would occur on the deposit-electrolyte interface rather than on the metal-electrolyte interface.[16]

Lin and Dexter[17] considered that the composition change, *i.e.*, more calcite than aragonite, is the reason for a slower formation rate at the low temperatures. Calcite is the predominant $CaCO_3$ phase at low temperatures, and Mg^{2+} ions inhibit calcite deposition in both the nucleation and crystal growth stages. In contrast, deposits can form at

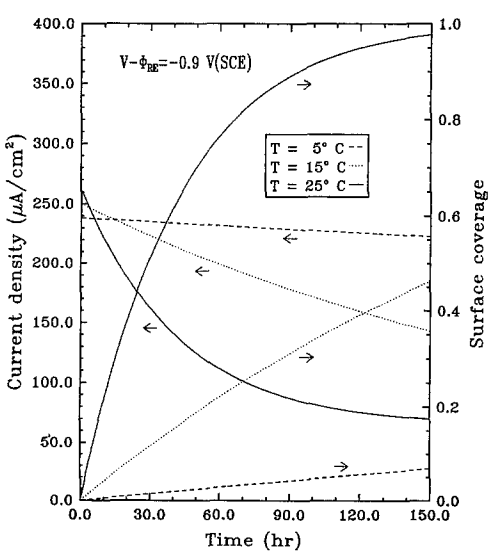

Fig. 5. Effect of temperature on the change in current density and surface coverage with time [−0.9 V (SCE), 50 rpm, 35 ppt salinity].

Table III. Transport properties and the concentrations of the components in seawater at salinities of 40, 35, and 30 ppt (temperature = 25°C).

Parameter	40 ppt	35 ppt	30 ppt
$c_{O_2} \times 10^{7}$ [a] (mol/cm^3)	2.05	2.11	2.18
$c_{H_2} \times 10^{10}$ [a] (mol/cm^3)	6.55	6.69	6.85
$c_{OH} \times 10^{9}$ [b] (mol/cm^3)	1.69	1.60	1.54
$c_{Mg^{2+}} \times 10^{5}$ [c] (mol/cm^3)	6.23	5.45	4.67
$c_{Ca^{2+}} \times 10^{5}$ [c] (mol/cm^3)	1.21	1.05	0.93
$c_{CO_3^{2-}} \times 10^{6}$ [b] (mol/cm^3)	0.24	0.21	0.18
$c_{HCO_3^-} \times 10^{6}$ [b] (mol/cm^3)	1.57	1.54	1.49
$c_{Na^+} \times 10^{4}$ [d] (mol/cm^3)	5.48	4.79	4.11
$c_{Cl^-} \times 10^{4}$ [c] (mol/cm^3)	6.37	5.58	4.78
$\rho_o \times 10^{3}$ [e] (kg/cm^3)	1.027	1.023	1.020
$\nu \times 10^{2}$ [e] (cm^2/s)	0.939	0.933	0.927

[a] Predicted from the equations in Ref. 28.
[b] Predicted from the equations in Ref. 29.
[c] Taken from Ref. 29.
[d] Taken from Ref. 29 and adjusted to meet the electroneutrality.
[e] Taken from Ref. 28.

higher temperatures, since aragonite is the stable phase and Mg^{2+} ions inhibit the nucleation but not the crystal growth stage of aragonite. However, some workers[19] claim that it is not the Ca/Mg ratio but the total deposits [$CaCO_3$ + $Mg(OH)_2$] that is the significant measure of the protectiveness of the calcareous deposits.

In the model used here $CaCO_3$ and $Mg(OH)_2$ are grown in a total mass and cannot be distinguished from each other. As mentioned above, it is the higher solubilty constant and the smaller kinetic parameters for $CaCO_3$ formation that reduce the formation rate of calcareous deposits in cold seawater.

Effect of Salinity

The salinity-dependent variables are listed in the Tables III and IV. The rest of the parameters in the model are assumed to be independent of the seawater salinity and are listed in Ref. 1. Figure 6 presents the results on the changes of current density and surface coverage with time for salinities of 30, 35, and 40 ppt.

The concentration of dissolved oxygen is reduced at higher salinity. This leads to a slightly lower initial current density as shown in Fig. 6. However, the concentrations of the reactive ions, such as Ca^{2+}, Mg^{2+}, and CO_3^{2-} are increased at high salinities. Since the transfer of species from the bulk solution to electrode surface is mass-transfer controlled, the concentrations of species on the electrode surface are dependent on the bulk concentrations. As a result, the formation rates of $CaCO_3$ and $Mg(OH)_2$ are slightly increased as the result of higher supersaturation as shown in Fig. 6.

Effect of Depth

The temperature, salinity, oxygen concentration, and pH at different depths in the northern half of the Gulf of Mexico, obtained from Ref. 20, are listed in Table V. The effects of pressure on the apparent solubility product and the apparent ionization constants of inorganic carbon equilibria were determined by using Ref. 21. The pressure dependence of the thermodynamic dissociation constant of water was adjusted by using Ref. 22.

Table IV. Parameters of the precipitation reactions and the homogeneous reaction at salinities of 40, 35, and 30 ppt (temperature = 25°C).

Parameter	40 ppt	35 ppt	30 ppt
$K_{sp,CaCO_3} \times 10^{13}$ [a] (mol^2/cm^6)	9.94	9.14	8.34
$K_{sp,Mg(OH)_2} \times 10^{19}$ [b] (mol^3/cm^9)	4.89	4.50	4.11
$K_{eq} \times 10^{-8}$ [a] (cm^3/mol)	0.90	0.84	0.76

[a] Predicted from Ref. 29.
[b] Taken from Ref. 27.

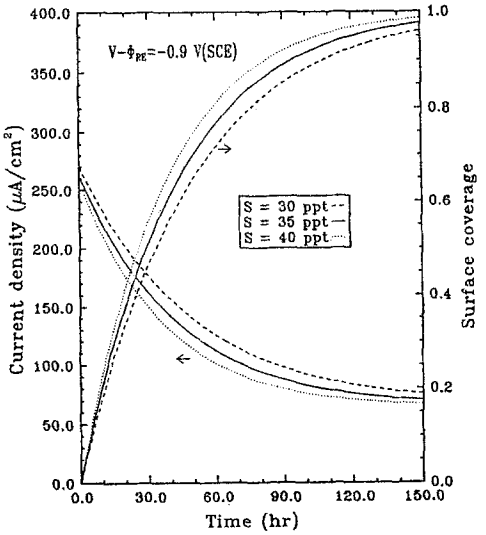

Fig. 6. Effect of salinity on the change in current density and surface coverage with time [−0.9 V (SCE), 50 rpm, 25°C].

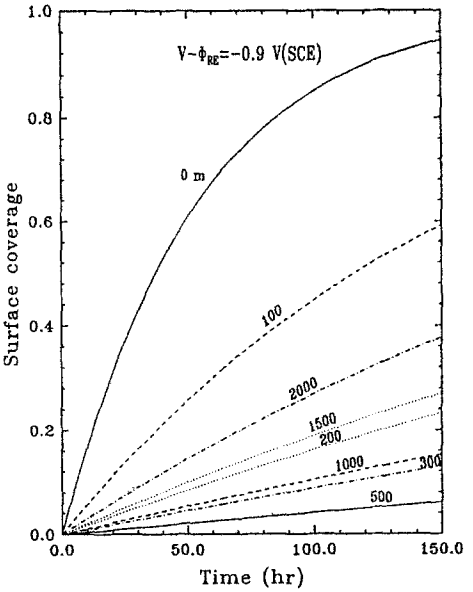

Fig. 7. Effect of depth on the change in surface coverage on cathodically protected steel in seawater with time [−0.9 V (SCE), 50 rpm].

Figure 7 shows the computed surface coverage rate on cathodically protected steel in seawater at different depths. The surface coverage of calcareous deposits decreases with depth; however, below 500 m, the surface coverage increases with depth in the seawater. The formation of calcareous deposits results in the decrease of the cathodic current density as shown in Fig. 8. The increase in the cathodic current density in the seawater deeper than 500 m is because a minimum value of oxygen content occurs between 400 and 500 m in the Gulf of Mexico. The predictions shown in Fig. 7 indicate that the rate of formation of calcareous deposits is much slower at various depths compared to the sea surface, and this finding agrees quantitatively with the previous report[23] that cathodically protected steel panels immersed in the ocean at a depth of 945 m at 4°C were not covered by calcareous deposits.

Figure 9 shows the variation of the supersaturation of $CaCO_3$ and $Mg(OH)_2$ with depth. $CaCO_3$ is supersaturated at depth, but its supersaturation decreases with depth because higher hydrostatic pressure and lower pH increase its solubility. The supersaturation of $Mg(OH)_2$ decreases first and is below 1.0 but increases with depth in seawater deeper than 500 m. This behavior is like the vertical distribution of oxygen content in the ocean.[20,24,25] The change in the supersaturation of $Mg(OH)_2$ in Fig. 9 suggests the close relationship between the formation of $Mg(OH)_2$ and the oxygen content in seawater. The results in Fig. 9 also imply that more $Mg(OH)_2$ would be formed in deep water than in shallow water. Our predictions are consistent with the work of England and Heidersback[26] which states that the primary deposits appear to be magnesium-rich minerals under high hydrostatic pressure (equivalent to a depth of 600 m).

Table V. Vertical distribution of temperature, salinity, oxygen concentration, and pH in the northern half of the Gulf of Mexico.

Depth (m)	T^a (°C)	S^a (ppt)	$c_{O_2} \times 10^{7\,a}$ (mole/cm^3)	pH^a
0	24	33.6	2.21	8.28
100	20	36.4	1.79	8.25
200	15	36.0	1.38	8.19
300	12	35.5	1.25	8.14
500	8	35.0	1.23	8.08
1000	5	34.9	1.84	8.09
1500	4	35.0	2.17	8.12
2000	4	35.5	2.29	8.13

[a] Taken from Ref. 20.

The predicted supersaturation values of $CaCO_3$ shown in Fig. 9 are higher than those in the literature.[27] This is because of the application of cathodic protection in the present work, whereas the results in Ref. 27 are based on the concentrations in the bulk solution. The application of cathodic current enhances the concentrations of OH^- and CO_3^{2-} ions on the steel surface and hence increases the supersaturation of $CaCO_3$.

Conclusions

The parametric studies presented here show that the applied potential and temperature influence the formation of calcareous deposits. The formation rate of calcareous deposits is increased at more negative applied potentials. Also, a high applied potential is favorable for the formation of $Mg(OH)_2$. The formation rate of calcareous deposits is relatively slow at low temperatures. The results show that the surface coverage on the electrode surface at 5°C is very small. And, even though the cathodic current density increases with rotation speed, the formation of calcareous deposits does not increase with rotation speed. The formation rate of calcareous deposits increases slightly when the

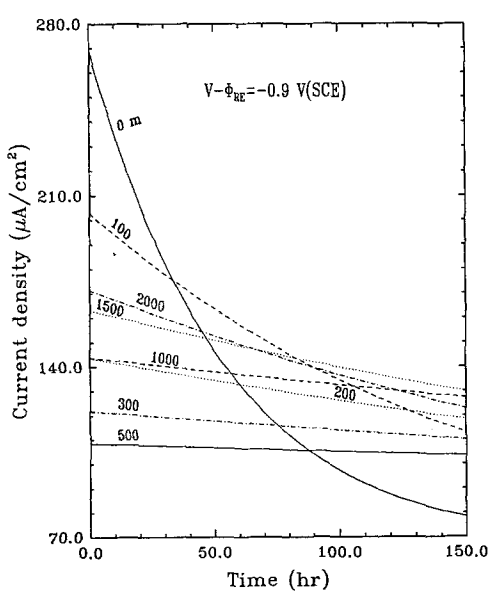

Fig. 8. Effect of depth on the change in current density on cathodically protected steel in seawater with time [−0.9 V (SCE), 50 rpm].

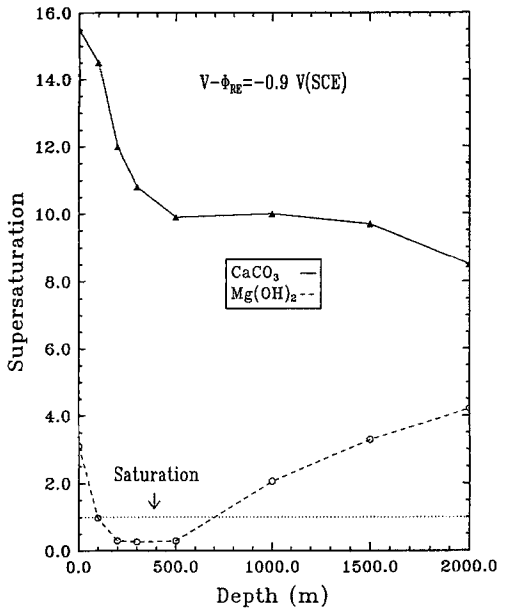

Fig. 9. Effect of depth on the change in the supersaturation of $CaCO_3$ and $Mg(OH)_2$ in seawater [−0.9 V (SCE), 50 rpm].

salinity is increased although the current density is decreased. Since all physical and chemical properties of seawater are dependent on depth. it can be considered as an important variable that influence the formation of calcareous deposits and their ability to lower the cathodic current density. The results show that the formation rate of calcareous deposits is much lower at various depths, compared to the sea surface. Also, the calcareous deposits formed in deep cold water would be expected to contain more $Mg(OH)_2$ than those formed in shallow water.

Acknowledgment

The authors are grateful for the financial support of this work by Offshore Technology Research Center (OTRC) at Texas A&M University.

Manuscript submitted Aug. 10, 1992; revised manuscript received Dec. 23, 1992.

Texas A&M University assisted in meeting the publication costs of this article.

LIST OF SYMBOLS

c_i	concentration of species i, mol/cm^3
D_i	diffusion coefficient of species i, cm^2/s
i_j	superficial current density for electrochemical reaction j, A/cm^2
i_T	total current density, A/cm^2
j_j	local current density for electrochemical reaction j, A/cm^2
k_{CaCO_3}	reaction rate constant for the precipitation reaction of $CaCO_3$, mol/cm^2 · s
$k_{Mg(OH)_2}$	reaction rate constant for the precipitation reaction of $Mg(OH)_2$, cm^7/mol^2 · s
K_{eq}	equilibrium constant for the homogeneous reaction (Eq. 5), cm^3/mol
$K_{sp,CaCO_3}$	apparent solubility product constant of $CaCO_3$, mol^2/cm^6
$K_{sp,Mg(OH)_2}$	apparent solubility product constant of $Mg(OH)_2$, mol^3/cm^9
m_{CaCO_3}	reaction order for the precipitation of $CaCO_3$
MW_{CaCO_3}	molecular weight of $CaCO_3$, g/mol
$MW_{Mg(OH)_2}$	molecular weight of $Mg(OH)_2$, g/mol
NR	number of electrochemical reaction
$R''_{Ca^{2+}}$	precipitation rate of Ca^{2+}, mol/cm^2 · s
$R''_{Mg^{2+}}$	precipitation rate of Mg^{2+}, mol/cm^2 · s
S	salinity, ppt
V	electrode potential, V
y_{RE}	thickness of diffusion layer, cm

Greek

δ	thickness of calcareous deposits, cm
ϵ_d	deposit porosity
ρ_{CaCO_3}	density of $CaCO_3$, g/cm^3
$\rho_{Mg(OH)_2}$	density of $Mg(OH)_2$, g/cm^3
ρ_o	density of seawater, kg/cm^3
ν	kinematic viscosity, cm^2/s
θ	surface coverage of calcareous deposits
Φ_{RE}	solution potential in bulk solution at the tip of the reference electrode, V

REFERENCES

1. J.-F. Yan, T. V. Nguyen, R. E. White, and R. B. Griffin, *This Journal,* **140,** 733 (1933).
2. M. G. Fontana, *Corrosion Engineering,* 3nd. ed., McGraw-Hill, Inc., New York (1986).
3. A. Turnbull and D. H. Ferriss, *Corros. Sci.,* **26,** 601 (1986).
4. K-M. Yin and R. E. White, *AIChE J.,* **36,** 187 (1990).
5. H. Gu, T. V. Nguyen, and R. E. White, *This Journal,* **134,** 2953 (1987).
6. T. Yeu, T. V. Nguyen, and R. E. White, *ibid.,* **135,** 1971 (1988).
7. W. E. Ryan, R. E. White, and S. L. Kelly, *ibid.,* **134,** 2154 (1987).
8. J. S. Newman, *Ind. Eng. Chem. Fundam.,* **7,** 514 (1968).
9. B. Carnahan, H. A. Luther, and J. O. Wilkes, *Applied Numerical Methods,* John Wiley & Sons, Inc., New York (1969).
10. H. A. Humble, *Corrosion,* **4,** 7, 358 (1948).
11. R. U. Lee and J. R. Ambrose, *ibid.,* **44,** 12, 887 (1988).
12. S. L. Wolfson and W. H. Hartt, *ibid.,* **37,** 2, 70 (1981).
13. J-F. Yan, Ph.D. Thesis, Texas A&M University, College Station, TX (1992).
14. K. P. Fischer and W. H. Thomason, Paper No. 577, *CORROSION/89,* National Association of Corrosion Engineers, Houston, TX (1989).
15. H. P. Hack and R. J. Guanti, *Mater. Perform.,* **28**(3), 69 (1989).
16. M. M. Kunjapur, W. H. Hartt, and S. W. Smith, *Corrosion,* **43,** 11, 674 (1987).
17. S-H. Lin and S. C. Dexter, *ibid.,* **44,** 9, 615 (1988).
18. H. R. England and R. H. Heidersbach, OTC 4365, 14th Annual Offshore Technology Conference, Houston, TX (1982).
19. J. E. Finnegan and K. P. Fischer, Paper No. 581, CORROSION/89, National Association of Corrosion Engineers, Houston, TX (1989).
20. A. D. Goolsby and B. M. Ruggles, *Corrosion,* **47,** 5, 387 (1991).
21. J. M. Edmond and J. A. Gieskes, *Geochim. Cosmochim. Acta,* **34,** 1261 (1970).
22. F. J. Millero and M. L. Sohn, *Chemical Oceanography,* CRC Press, Boca Raton, FL (1992).
23. L. J. Waldron, M. H. Peterson, and B. F. Brown, NRL Memorandum report No. 1242.
24. S. C. Dexter and C. Culberson, *Mater. Perform.,* **19,** 9, 16 (1980).
25. J. Burton, *Chem. Indust.,* **16,** 550 (1977).
26. H. R. England and R. H. Heidersbach, CH1685-7, 1981 IEEE (1981).
27. W. H. Hartt, C. H. Culberson, and S. W. Smith, *Corrosion,* **40,** 11, 609 (1984).
28. M. Whitfield and D. Janger, *Marine Electrochemistry,* John Wiley & Sons, Inc., New York (1981).
29 G. Skirrow, in *Chemical Oceanography,* Vol. 2, 2nd. ed., J. P. Riley and G. Skirrow, Editors, Academic Press, Inc., New Yrok (1975).,
30. J. H. Simpson and H. Y. Carr, *Phys. Rev.,* 2nd Series, 1201 (1958).
31. Y.-H. Li and S. Gregary, *Geochim. Cosmochim. Acta,* **38,** 703 (1974).